Annals of Glaciology 3 1982

OCEANOGRAPHIC OBSERVATIONS FROM GEORGE VI ICE SHELF, ANTARCTIC PENINSULA

by

P. W. Lennon, J. Loynes, J. G. Paren and J. R. Potter

(British Antarctic Survey, Natural Environment Research Council, Madingley Road, Cambridge CB3 0ET, England)

ABSTRACT

Summer profiles of sea-water temperature, salinity and flow were obtained on George VI Ice Shelf near its northern ice front. At each depth, temperature salinity and density show little variation between sites. Their respective variation to 250 m depth confirms a linear temperature-salinity dependence. This is the first place in the world where observations confirm precisely the form of the T-S diagram predicted for fresh ice melting in sea-water. Both tidal and residual flow are small, except at the western margin of the ice front, where a strong outflow is concentrated immediately beneath the ice shelf. The observations lead to a simple circulation model for the ice-shelf regime. Warm Deep Water flows southwards into George VI Sound, replacing the colder water that spreads northwards in the surface outflow. Thermohaline exchanges beneath the ice shelf determine the salinity profile, which itself provides evidence of upwelling. Estimates can be made of the basal melt rate of the ice shelf. The rates vary from around 10 m a^{-1} at the ice front to an average value for the ice shelf of order 1 m a^{-1}. The average value is consistent with earlier estimates from surveys of ice-shelf strain.

INTRODUCTION

The Antarctic Peninsula is a major oceanographic and climatic barrier that projects into the Southern Ocean and separates the Weddell Sea from the South Pacific Ocean. In crossing the peninsula from west to east in latitude 70°S, mean air temperatures at sea-level fall by 7°C and maximum deep sea-water temperatures by 1°C. The west coast of the peninsula is the warmest part of mainland Antarctica, and there are no ice shelves north of latitude 67°S. The objective of our study was to determine the oceanographic environment close to the climatic limit for ice shelves. George VI Ice Shelf is the largest ice shelf on the west coast of the Antarctic Peninsula and was presumed to have a high rate of basal melting. A comparison could then be made with data from the continental shelves off Ronne/Filchner and Ross ice shelves.

PHYSICAL SETTING

George VI Sound is a channel extending for 500 km between roughly parallel flanks of land from Marguerite Bay in the north to Ronne Entrance on the Bellingshausen Sea (Fig.1(a)). The bottom topography of the channel is highly irregular and ranges in depth from 400 to 1 000 m. The deep channel extends north into Marguerite Bay where it cuts into the ≈500 m deep continental shelf.

George VI Ice Shelf extends for almost the full length of the sound, covers about 26 000 km^2, and has northern and southern ice fronts totalling 100 km in length. The thickness of the ice shelf varies from 100 m near the northern ice front to a maximum of 500 m in latitude 72°50'S.

Ronne Entrance is an area of open water that generally remains ice-free throughout the year. By contrast, the northern ice front has one very small polynya (≈15 km^2) at its western margin during the summer months, but is generally ice-bound.

The observational sites of the present investigation all lie within 13 km of the northern ice front (Fig.1(b)). In this area, aligned roughly parallel to the ice front, there are rifts which penetrate through the ice shelf. Recent evidence suggests that the rifts are an intermediate stage in the calving process. From field and satellite observations, it is clear that the position of the northern ice front has retreated southwards during the period January 1977 to January 1979 (Fig.1(b)). The present (1981) ice front was an ice-shelf rift of January 1977. The rifts are typically 300 m wide and 5 km long, with a floor of sea ice 1 to 5 m thick in summer. Access to the sea was found through holes and small cracks in fast ice off the ice front and also in rifts.

PREVIOUS OBSERVATIONS

Detailed surveys of ice strain on George VI Ice Shelf have been used to calculate basal melt rates on the assumption of steady-state conditions (Bishop and Walton 1981). Results from 20 points on the ice shelf range from 0.5 to 8.0 m a^{-1} of ice. At only two points does the basal melt rate exceed 2 m a^{-1}.

Earlier measurements of sea temperature and in situ salinity were made through two naturally occurring access holes, termed lake sites, on the eastern margin of George VI Ice Shelf (Bishop and Walton 1981). At Carse Point (70°15'S, 68°12'W, 40 km south of the ice front) where the ice-shelf thickness is ≈100 m, temperatures were above freezing at all depths. However, further south at Hobbs Pool (71°18'S, 67°35'W, 160 km south of the ice front) where the ice-shelf thickness is ≈200 m, the water temperature was close to the freezing point within the draught of the ice shelf. The upper 70 m was essentially fresh water. Beneath the ice shelf, temperature and salinity increased to the sea floor.

https://doi.org/10.3189/S0260305500002731 Published online by Cambridge University Press

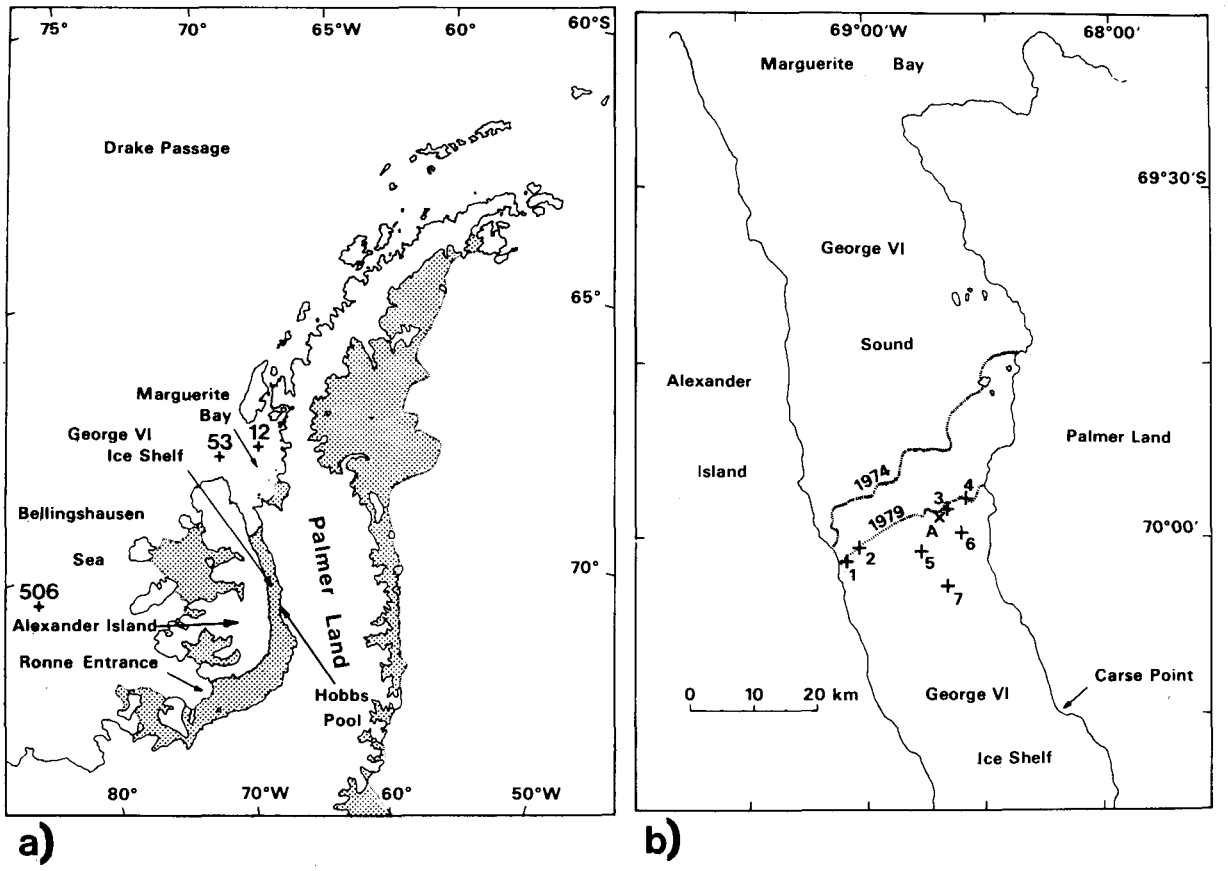

Fig.1. The location of George VI Ice Shelf. (a) The crosses indicate the positions of hydrographic stations used in Figure 3. (b) The crosses and numbers 1 to 7 indicate field sites visited in the period 1979 to 1981. The cross marked with letter A indicates a field site visited in 1977.

Tidal observations have been made at three lake sites on George VI Ice Shelf and analysed for harmonic constants (Cartwright 1980). Near the northern ice front, the amplitudes of the tidal variations in sea level and current are typically 0.5 m and 75 mm s^{-1} respectively. In Marguerite Bay, and near the northern ice front, the tides are dominated by a strong solar diurnal component.

INSTRUMENTATION AND METHODS

National Institute of Oceanography (NIO) water-sampling bottles carrying mercury reversing thermometers were used at standard depths down to the sea-floor. Using two sampling bottles simultaneously, the deepest profiles took six hours to complete. The error in temperature measurements is ±0.01°C and a bench salinometer for the sea-water analysis gives an error of ±0.004°/oo in salinity.

For measurement of in situ temperature and salinity in conjunction with current speed and direction, several Aanderaa RCM4 meters were used. These instruments take measurements at a pre-selected time interval ranging from 30 s to 2 h. The current speed measurement is cumulative during the time interval. The Savonius rotor has a threshold of 15 mm s^{-1} and direction measurements are accurate to ±5°. The standard model resolves temperature to 0.02°C and salinity to 0.10°/oo. We also used several non-standard models to provide improved resolutions of 0.01°C for temperature and 0.02°/oo for salinity. For instantaneous and continuous measurements of current speed, an electromagnetic current meter was employed with zero speed threshold and an accuracy of ±5 mm s^{-1}.

CURRENTS

At site 1, near the western margin of the sound, a strong current of up to 300 mm s^{-1} and vertical extent of over 100 m was found immediately below the ice shelf. This current is very stable in direction and runs outward along the axis of the sound into the recurring polynya. Elsewhere, currents are very small for the area underlying the northern ice front, and their character conforms to that expected for tidal currents.

TEMPERATURE AND SALINITY

Temperature-salinity diagram

Figure 2 is the temperature-salinity (T-S) diagram using measurements made with NIO water-sampling bottles at and below 10 m depth. The results shown are for five sites (1, 3, 5, 6, and 7 of Figure 1) in George VI Sound. The points fall within a narrow envelope, and the more scattered are equally divided between the profiles at different sites.

With only few exceptions, the points confirm a single T-S dependence within the precision of the measurements of temperature and salinity. Linear relationships observed on T-S diagrams are evidence of the mixing of two water masses; the kinetics of the process determine the depth at which a given pair of T-S values are found. First impressions of Figure 2 suggest that the water sources are located at the sea surface and near the sea bed, since one line appears to dominate the whole T-S profile. However, on detailed analysis of the data, two distinct breaks of slope are detected, which exceed experimental uncertainty. The first break of slope occurs where the

https://doi.org/10.3189/S0260305500002731 Published online by Cambridge University Press

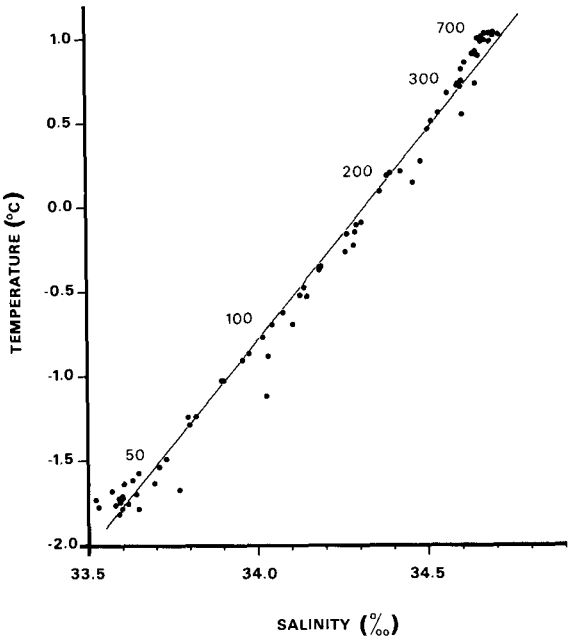

Fig.2. The temperature-salinity (T-S) diagram for 5 sites in George VI Sound. Numbers beside the data points indicate the depth in metres. The gradient of the straight line is 2.47°C °/oo^{-1}.

temperature is -0.88°C, the salinity is 34.0°/oo and the depth is 85 m; the second break of slope occurs where the temperature is +0.50°C, the salinity is 34.5°/oo and the depth is 250 m. From 10 to 85 m depth, the gradient of the T-S line is 2.23 ± 0.10°C °/oo^{-1}. Between 85 and 250 m depth, the gradient is 2.46 ± 0.06°C °/oo^{-1}. These breaks of slope appear to mark the boundaries between regimes of different character. The occurrence of the boundary at 85 m depth is strong evidence that the bottom of the ice shelf lies at this depth, implying a total ice-shelf thickness of ≈100 m.

The theoretical characteristic T-S diagram for ice melting in sea-water may be deduced by a simple argument. Temperature and salinity are clearly interrelated since, as it melts, ice cools sea-water by the absorption of latent heat and, at the same time, reduces the salinity. The gradient of the T-S diagram can be determined directly from the conservation of heat and salt, as Gade (1979) and Griesman (1979) have shown. They consider the heat and salt balance for 1 kg of ice melting completely into M kg of water at temperature T and salinity S. After mixing thoroughly, the water parcel of (M+1) kg has a salinity of S+δS and a temperature of T+δT.

From the analysis of Gade (1979), the heat balance equation is,

$$\delta T = -(L_f C_w^{-1} + (T - T_f) + (T_f - T_0)\, C_i C_w^{-1})/(M + 1),$$

where T_f is the freezing temperature corresponding to the salinity at the level of the bottom of the ice shelf, L_f is the latent heat of fusion corresponding to the temperature T_f, T_0 is the ice temperature 10 m below the top surface of the ice shelf, and C_i and C_w are respectively the specific heats of ice and sea water.

The salt balance determines that

$$\delta S = -S/(M + 1).$$

The resulting steady-state gradient of the T-S diagram is therefore

$$dT/dS = (L_f C_w^{-1} + (T - T_f) + (T_f - T_0)\, C_i C_w^{-1})\, S^{-1}. \quad (1)$$

For the range of salinity and temperature observed in Figure 2, equation 1 predicts a theoretical value for dT/dS within the range 2.47±0.05°C°/oo^{-1} depending on the values chosen for the parameters L_f and T_0. L_f must be less than the latent heat of fusion at 0°C (333.6 kJ kg^{-1}), yet data are sparse and apparently inconsistent for T<0°C. Interpolating the data for T_f = -1.94°C gives L_f in the range 324 to 330 kJ kg^{-1}, the upper value probably being more realistic. Bishop and Walton (1981) reported T_0 in the range -2°C to -5°C north of 70°30'S on George VI Ice Shelf, although colder ice temperatures prevail further south from the ice front. The specific heat values are C_i = 2.09 kJ kg^{-1} °C^{-1} and C_w = 3.99 kJ kg^{-1} °C^{-1}.

On Figure 2 a straight line has been drawn with the theoretical gradient of 2.47°C°/oo^{-1}, but the position of the line is arbitrary. There is good agreement in gradient between theory and observations from 85 m until around 250 m depth; thus, ice melting totally dominates the salinity and temperature profiles in the 85 to 250 m range. This is the first known example where there has been clear confirmation of the theoretical gradient. Beneath the Ross Ice Shelf, for example, dT/dS = 0.65°C°/oo^{-1} (Jacobs and others 1979), so other processes may constrain the gradient, probably due to the low basal melt rate.

Profiles of salinity and temperature at the northern ice front

At each depth, temperature, salinity and density show small but observationally significant variations between sites. Averaging the salinities and temperatures at the depths common to the five profiles, characteristic profiles for the northern ice-front area are obtained. These are shown in Figure 3, together with the profiles of the closest hydro-

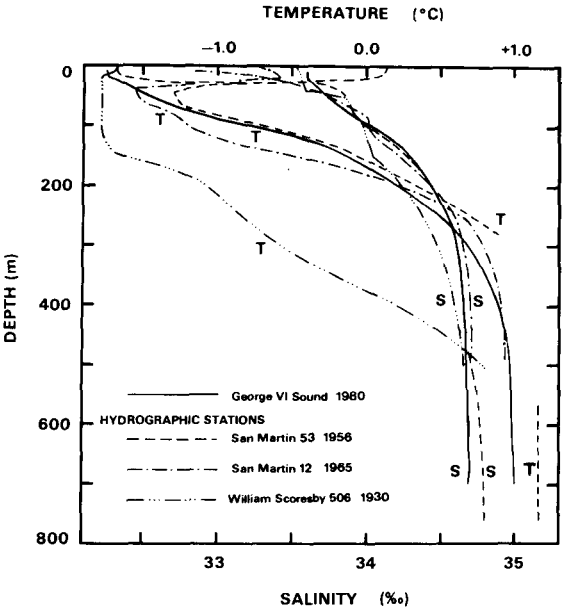

Fig.3. The variation of temperature T and salinity S with depth for four sites around Alexander Island. To obtain the George VI Sound result, data from sites 1, 3, 5, 6 and 7 (Fig.1) were averaged. Ship data are from hydrographic surveys: San Martin station 53 (1956) and station 12 (1965), William Scoresby station 506 (1930). These stations are listed in US Naval Oceanographic Data Center (unpublished), and are the closest available to the ice fronts.

https://doi.org/10.3189/S0260305500002731 Published online by Cambridge University Press

graphic stations obtained from a World Data Centre (US Naval Oceanographic Data Center unpublished).

Before considering the implications of the average profile for the sites, we will consider the significant but small differences between them. Concentrating only on depths lying below the level of the bottom of the ice shelf, the standard deviations for temperature and salinity vary from 0.16°C and 0.081°/oo at 100 m depth to a minimum of 0.003°C and 0.004°/oo at 400 m depth. A feature of the variations common to all depths is that they are equivalent to a similar vertical movement along the averaged characteristic profile for the ice front. Corresponding to the standard deviations in the 100 to 400 m depth range, the movement is 14 m for salinity and 7 m for temperature. A series of six temperature profiles at site A at different states of the tide give an equivalent vertical movement of 4.5 m for temperature over the same depth range; the greatest temperature fluctuations occurred at 90 m depth, presumably near the bottom of the ice shelf where the maximum fluctuation was 0.17°C and the standard deviation 0.09°C. A five month mooring of an Aanderaa RCM4 current meter at 150 m depth at site 5 showed no progressive cooling or increase of salinity towards midwinter, yet fluctuations dominated the entire record, ranging within ±0.17°C and ±0.085°/oo.

In the open ocean, density profiles at neighbouring stations are used to determine the steady-state current flow that is required to maintain them in the absence of frictional forces. For this geostrophic flow, dynamic height anomalies are calculated from the profiles. We have performed such an analysis, and found the dynamic height anomalies poorly correlated with position (correlation coefficient around 0.6 across the sound, around 0.3 in from the ice front). The analysis shows that fluctuations, which are evidence of turbulent mixing or internal waves, are of overriding significance when trying to determine those time independent deviations between sites due to the geometrical constraints of the local environment. We therefore accept the mean profile for the five sites as an average of position and tide for comparison with summer profiles at other hydrographic stations.

CIRCULATION IN GEORGE VI SOUND AND MARGUERITE BAY

Warm Deep Water provides the only sustained southward flow in the Southern Ocean, replacing the cold water that spreads northwards in the surface and bottom layers. Bottom Water is not found on the continental shelf of Marguerite Bay, since Warm Deep Water extends to the sea floor, where its maximum temperature and salinity are observed. Comparing observations near the sea floor we find that station 12 is 0.08°/oo less saline and 0.22°C cooler than station 53 (Fig.3). George VI Sound is 0.09°/oo less saline and 0.15°C cooler than station 53. These observations suggest that Warm Deep Water becomes fresher and cooler as it moves into Marguerite Bay. Non-tidal currents in Marguerite Bay are very small when calculated from the three profiles by geostrophic arguments. A level of zero net flow is to be expected at the boundary of the surface water and Warm Deep Water if these water masses flow in opposite directions. The boundary can be used as the reference level of zero net flow in the geostrophic flow calculation. Assuming it occurs between 200 and 300 m depth, values can be calculated for the current speed averaged from the surface to the reference level; they are all less than 1 mm s^{-1}. This is the component which is perpendicular to the line joining stations. The position of the three stations is such that a clockwise gyre could be present in Marguerite Bay without being revealed.

George VI Sound is ice-covered, which discounts the possibility of a wind-driven circulation. Moreover, tidal and residual currents are small. All this suggests that thermohaline circulation may be dominant under the ice shelf. A steady-state temperature or salinity field should satisfy the eddy diffusivity relationship

$$\underline{V}.\nabla F = \underline{K}.\nabla^2 F, \qquad (2)$$

where F is the property field, $\underline{V}$ the velocity field, and $\underline{K}$ the vector eddy diffusivity.

For the analysis we chose orthogonal coordinates with the X axis parallel to the base of the ice shelf along the axis of the sound and the Z axis downward. We have evidence that, in the 150 m-thick water layer directly under the ice shelf, isotherms are parallel to the bottom surface. This is an unexpected result and comes from the observation of temperature profiles at Hobbs Pool and Carse Point, which in the same layer are similar to the mean profile at the northern ice front. Hobbs Pool is the crucial site. With respect to depths measured from the sea surface, the Hobbs Pool profiles are in broad agreement with the ice-front profile once a depth adjustment of 70 ± 15 m is made. Hobbs Pool temperatures are close to the freezing point to a level of about 165 m where minimum temperatures are observed; they then increase abruptly to greater depths. 165 m is the presumed level of the bottom of the ice shelf, which exceeds that at the northern ice front by ≈80 m.

Equation 2 can now be written

$$w\partial T/\partial Z = K_z \partial^2 T/\partial Z^2, \qquad (3)$$

where w is the vertical component of velocity. This simplified form has been used by Gade (1979) as the basis for theoretical models of salinity and temperature profiles beneath ice shelves. Figure 4 displays $\partial T/\partial Z$ and $\partial S/\partial Z$ logarithmically against depth; $\partial S/\partial Z$ has been multiplied by 2.46°C °/oo^{-1} (the empirical gradient of the T-S diagram) so that both profiles can be displayed together with the same scale. A

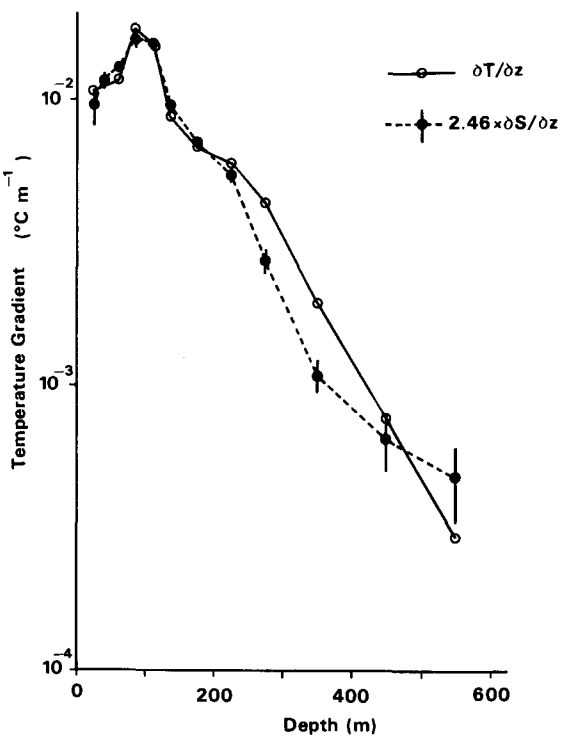

Fig.4. The average temperature gradients for sites 1, 3, 5, 6 and 7 plotted logarithmically against depth. In addition, the average salinity gradients are plotted multiplied by 2.46°C °/oo^{-1}. The possible errors in 2.46 $\partial S/\partial Z$ are given for a 0.004°/oo uncertainty in each salinity determination.

https://doi.org/10.3189/S0260305500002731 Published online by Cambridge University Press

logarithmic presentation has been used, since, when w/K_z is constant, there is a straight line solution for $\partial T/\partial Z$ from Equation 3:

$$\partial T/\partial Z = A \exp(wZ/K_z). \qquad (4)$$

Within the draught of the ice shelf, $w>0$, and flow is downwards; at the base of the ice shelf, $\partial^2 T/\partial Z^2 = 0$, $w = 0$, and flow is wholly parallel to the bottom surface of the ice shelf; within the remainder of the water column, there is an upwelling ($w<0$), which is variable in w/K_z for the top 150 m where temperature and salinity are interrelated. Values of w/K_z (the gradient of the $\partial T/\partial Z$ and $\partial S/\partial Z$ plots in Figure 4) can be used to calculate w, once K_z is known. In the depth range 100 to 250 m, the maximum value of $w/K_z = -(50\ m)^{-1}$ and the average value of $w/K_z = -(90\ m)^{-1}$. The $\partial T/\partial Z$ plot indicates that at greater depths $w/K_z = -(102\ m)^{-1}$ and is approximately constant. Thus, at depths greater than 100 m, an average value of $w/K_z = -(100\ m)^{-1}$ can be inferred at at the ice front. At Hobbs Pool, 160 km to the south a similar temperature profile is observed. Therefore, the upwelling rate appears constant over at least one-fifth of the area of the ice shelf.

Outflow

The surface outflow from the sound is concentrated at the western coastline. To examine this flow, an electromagnetic current meter was deployed at two sites (sites 1 and 2 of Figure 1) 3 and 6 km respectively from the western margin. The profiles obtained from sampling periods of 1 to 30 h are shown in Figure 5. Once account is taken of tidal currents and

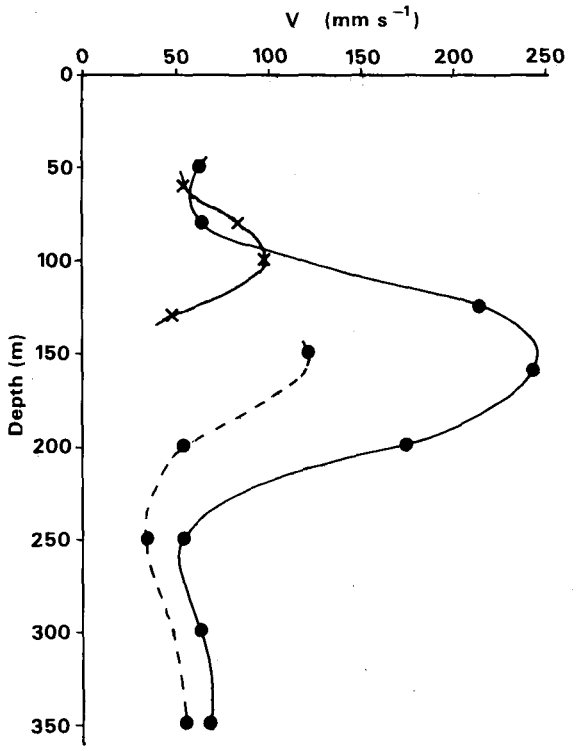

Fig.5. Mean current flow as a function of depth for site 1 (circles) and site 2 (crosses). Data collected in 1979-80 season (dashed line) and 1980-81 season (solid line).

the presence of the ice shelf to ~85 m depth, certain conclusions can be drawn. At site 1, the strong outflow dominates the upper 100 to 150 m of the water column beneath the ice shelf; the form of the profile is similar for the two seasons' measurements despite a variation in current strength. At site 2, the current is weaker, extends vertically only 60 m and has its maximum outflow at 100 m depth. Since site 2 was 100 m north of the ice front, the lesser depth of the current may be a result of upwelling at the ice front.

The profiles show that the current decreases both in velocity and thickness to the east, almost disappearing 6 km from the margin. This suggests that the current is a buoyant outflow collected to the west by the Coriolis force. Our hypothesis is supported by a calculation which shows that the horizontal extent of the outflow is approximately equal to the Rossby radius of deformation, λ, which gives a length scale for motion controlled by Coriolis effects (Pond and Pickard 1978). $\lambda = (g\Delta\rho D/\rho)^{0.5}/f$, where g is the acceleration of free fall, $\Delta\rho$ the density difference between the water type which constitutes the current and the water type underlying it, D the current thickness, ρ the density and f the Coriolis parameter. The value calculated for the western boundary current is 5 km.

Numerical integration for a flow averaged between the two profiles at site 1 gives an estimate for the outflow at the western boundary. The value is $5 \times 10^4\ m^3\ s^{-1}$.

Basal melting of George VI Ice Shelf

A speculative calculation can be made of the basal melt rate for George VI Ice Shelf. We take 250 m depth as the level separating the inflow and outflow, and consider that, outside the western boundary current, outflow is negligible. Furthermore, we assume that the circulation in the north of the sound is independent of that in Ronne Entrance. The temperature data from station 506 (Fig.3) show that the water properties in the Bellingshausen Sea are very different from those in the northern area of George VI Sound and consequently we do not expect the mechanisms governing the northern area to extend very far south.

In principle, we have enough information to calculate the basal melting rate. We know the approximate velocity-with-depth relationship for the outflow. We also know the temperature and salinity dependence with depth for the outflow. Integrating over depth, the product of salinity and velocity gives the total salt flux of the outflow. Similarly, integrating the product of temperature and velocity gives the temperature flux. Dividing these fluxes by the velocity flux gives the mean salinity and temperature of the outflow. Comparison of these quantities with the salinity and temperature of Warm Deep Water, from which the outflow is ultimately derived, yields the percentage of the outflow supplied by ice melt. Both salinity and temperature comparisons have been done; each shows independently that the approximate proportion of the outflow supplied by melting ice is 1%. If q is the proportion of the ice-shelf area (26 000 km^2) with sea connection to Marguerite Bay, then the mean basal melt is $0.6/q\ m\ a^{-1}$. For example, setting $q = 1/3$, the melt rate is $1.8\ m\ a^{-1}$. This value of q corresponds to an area extending from the northern ice front to a line equidistant from the two ice fronts.

The outflow must also balance the thermohaline upwelling over the same area. The vertical velocity w is not known absolutely; only w/K_z is known, and K_z, the eddy diffusivity, is a poorly known parameter in an ice-shelf regime. It is a property of the flow, and should be stability- and velocity-dependent. Jacobs and others (1979) followed earlier practice and chose a value of $1 \times 10^{-4}\ m^2\ s^{-1}$ for the regime beneath the Ross Ice Shelf, whilst Gade (1979) deduced a value between 20×10^{-4} and $30 \times 10^{-4}\ m^2\ s^{-1}$ from an analysis of a T-S diagram from the same area. If the proportion of the ice melt in the outflow is 1%, then the upwelling velocity required to sustain a melt of $1.8\ m\ a^{-1}$ is $180\ m\ a^{-1}$. For $w = 10^{-2}\ K_z$, this implies $K_z = 6 \times 10^{-4}\ m^2\ s^{-1}$, which is within the range quoted for the Ross Sea. Thus, a basal melt of $2\ m\ a^{-1}$ is a possible solution to the oceanographic observations if the circulation under the ice shelf

https://doi.org/10.3189/S0260305500002731 Published online by Cambridge University Press

is restricted. It is compatible with previous glaciological observations (Bishop and Walton 1981). Alternative estimates of basal melt rate can be made using the criterion of temperature elevation above the freezing point at the bottom of the ice shelf. The temperature elevation increases with depth, from a minimum of 0.11°C at 10 m depth to a maximum of 3.44°C at 700 m. At 85 m (our estimated depth of the bottom surface of the ice shelf), it is 1.06°C. Based on the laboratory experiments of Russell-Head (1980), this temperature elevation should result in a basal melt of 7 m a^{-1}. According to the analysis of iceberg disintegration rates by Budd and others (1980), a melt rate of between 8 and 22 m a^{-1} is obtained by extrapolation. Gill (1973) has shown how the melt rate beneath an ice shelf should be related both to the current velocity and to the basal temperature elevation. The theoretical relationship is

$$\text{melt rate} = c_H C_w \Delta T \, V / L_f \qquad (5)$$

where c_H is a theoretically derived constant, ΔT is the basal temperature elevation, and V is the current velocity. On applying the theoretical formula to estimates of the melt rate deduced from glaciological observations at the ice fronts of Brunt (3 m a^{-1}), Ronne (10 m a^{-1}), and Ross (0.8 m a^{-1}) ice shelves Gill concluded that the stabilizing influence of melt water at the ice/water interface caused the theoretically derived constant in the formula to be reduced to about one-tenth. By similarly applying a tenfold reduction, a melt rate of 7 m a^{-1} is obtained for the northern ice front for the mean current of 50 mm s^{-1} measured over a period of five months.

CONCLUSION

This paper has presented measurements made at one ice front of an ice shelf near its climatic limit. The observed temperature-salinity relationship for water at the ice front has been shown to agree closely with the thermodynamic theory governing ice melting over saline water. A thermohaline model of upwelling has been developed and is consistent with observations. To estimate basal melt rates requires certain assumptions. If the circulation beneath the ice shelf is divided into two separate systems by a line equidistant from the northern and southern ice fronts, an approximate basal melt rate of 1.8 m a^{-1} is obtained for the northern system. The basal melt rate at the ice front is expected to be greater than elsewhere and is estimated to be around 10 m a^{-1}.

Further work will be directed at increasing the available data on the circulation and testing the assumptions made in order to improve confidence in the model. The authors also expect to draw comparisons with the work of Huppert and Turner (1978) and Huppert (1980), and to examine the implications of any differences.

REFERENCES

Bishop J F, Walton J L W 1981 Bottom melting under George VI Ice Shelf. *Journal of Glaciology* 27(97): 429-447

Budd W F, Jacka T H, Morgan V I 1980 Antarctic iceberg melt rates derived from size distributions and movement rates. *Annals of Glaciology* 1: 103-112

Cartwright D E 1980 Analyses of British Antarctic Survey tidal records. *British Antarctic Survey Bulletin* 49: 167-179

Gade H G 1979 Melting of ice in sea water: a primitive model with application to the Antarctic ice shelf and icebergs. *Journal of Physical Oceanography* 9(1): 189-198

Gill A E 1973 Circulation and bottom water production in the Weddell Sea. *Deep-Sea Research* 20(2): 111-140

Greisman P 1979 On upwelling driven by the melt of ice shelves and tidewater glaciers. *Deep-Sea Research* 26(9A): 1051-1065

Huppert H E 1980 The physical processes involved in the melting of icebergs. *Annals of Glaciology* 1: 97-101

Huppert H E, Turner J S 1978 On melting icebergs. *Nature* 271(5640): 46-48

Jacobs S S, Gordon A L, Ardai J L Jr 1979 Circulation and melting beneath the Ross Ice Shelf. *Science* 203(4379): 439-443

Pond S, Pickard G L 1978 *Introductory dynamic oceanography*. New York, Pergamon Press

Russell-Head D S 1980 The melting of free-drifting icebergs. *Annals of Glaciology* 1: 119-122

US Naval Oceanographic Data Center Unpublished. Data extracted from USNODC file of October 1974. Inventory of the Antarctic. Obtainable from World Data Centres (Oceanography)

https://doi.org/10.3189/S0260305500002731 Published online by Cambridge University Press